Direction-of-Arrival Angle and Position Estimation for Extended Targets Using Multichannel Airborne Radar Data

Sushil Kumar Joshi, *Member, IEEE*, Stefan V. Baumgartner, *Senior Member, IEEE*, André Barros Cardoso da Silva, *Member, IEEE*, and Gerhard Krieger, *Fellow, IEEE*

***Abstract*— Direction-of-arrival (DOA) angle estimation is a prerequisite for projecting the airborne radar-based target detections to ground via a geocoding operation. Most state-of-the-art DOA angle estimation methods assume one detection per target. These methods cannot be applied one-to-one on extended targets like ships because individual ships in high-resolution data are generally composed of several distinct radar detections. In this letter, four methods for estimating the DOA angle for extended targets are formulated and discussed. The performance of the proposed methods is assessed by using simultaneously acquired automatic identification system (AIS) data of real ships. Radar data from the DLR's multichannel airborne digital beamforming synthetic aperture radar (DBFSAR) system are used to demonstrate the robustness and applicability of the proposed methods in real maritime scenarios.**

***Index Terms*— Airborne radar, direction-of-arrival (DOA) estimation, maritime safety, radar detections.**

I. Introduction

FREQUENT ship monitoring is essential for ensuring maritime safety and security. Operational state-of-the-art surveillance systems that are used for this task are the automatic identification system (AIS), marine or shipborne radars and coastal surveillance radars [1]. Not all ships, especially the smaller ones, are equipped with AIS transponders and marine radars are not sufficient for maritime surveillance because of their limited range. Coastal radars have a longer range because they are installed at higher altitudes such as hills, but their surveillance area is generally limited to coastal regions. Hence, ships on open sea, far away from the coast cannot be detected. Air- or spaceborne radar sensors can provide additional support to these existing systems and can fill the maritime surveillance gaps. Besides their all-weather and day-night acquisition capabilities, airborne radars have the ability to collect data with very high resolution and, unlike space-based radars, they also allow for shorter revisits and longer observation times on both the land and the ocean surfaces [2].

Airborne radar data acquired using multiple receiving (RX) channels are exploited to compute the direction-of-arrival (DOA) angle of the detected target. With the known DOA angle and the aircraft's navigation parameters, the targets can be mapped on ground so that the target's geographical coordinates can be obtained [3] and compared with the simultaneously acquired AIS data for validation purposes [4].

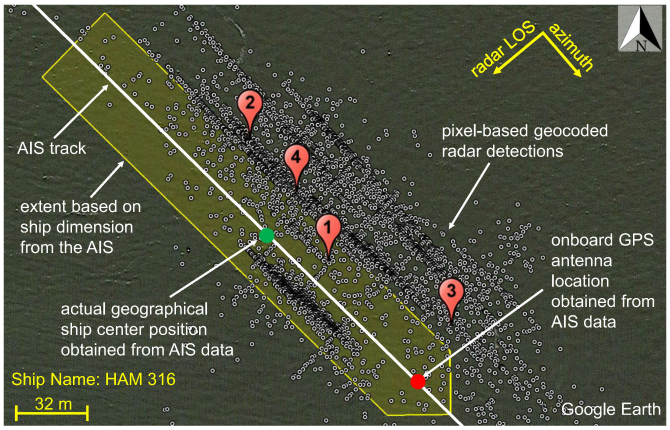

Fig. 1. Geocoded radar-based detections obtained from a real ship at a specific time instant using real multichannel airborne radar data. Due to the side-looking acquisition geometry of the radar and the ship height, the detections are slightly displaced toward the radar in its line-of-sight (LOS) direction. Geographical positions 1, 2, 3, and 4 in the figure are based on the proposed methods discussed in Section IV.

For estimating the DOA angle, the targets in classical moving target indication (MTI) algorithms are assumed as point-like targets. This assumption is certainly valid for smaller targets (e.g., road vehicles) in low-resolution data where each target of interest is within a single radar resolution cell [5]. However, in high-resolution data targets like ships usually appear as extended targets occupying more than a single resolution cell [6]. As a result, state-of-the-art DOA angle estimation methods, which are designed for point-like targets, cannot be applied directly to extended targets even if their corresponding pixel-based detections are already clustered [7].

An example is shown in Fig. 1, where the ship HAM 316 (cf. Table II for specifications) has more than 4000 radar-based detections at a specific time instant. It can be seen from the figure that the pixel-based geocoded detections obtained from the ship are spatially distributed. This is because each detection is mapped on ground according to a specific DOA angle. The goal is to determine a single DOA angle, so that a single position of the extended target on ground can be determined. By doing this, extended target tracking becomes easier.

Manuscript received September 11, 2021; revised January 28, 2022; accepted February 17, 2022. Date of publication February 28, 2022; date of current version March 21, 2022. This work was supported by the German Academic Exchange Service (DAAD) under Grant 57265855. *(Corresponding author: Sushil Kumar Joshi.)*

The authors are with the Radar Concepts Department, Microwaves and Radar Institute, German Aerospace Center (DLR), 82234 Weßling, Germany (e-mail: sushil.joshi@dlr.de).

Digital Object Identifier 10.1109/LGRS.2022.3155245

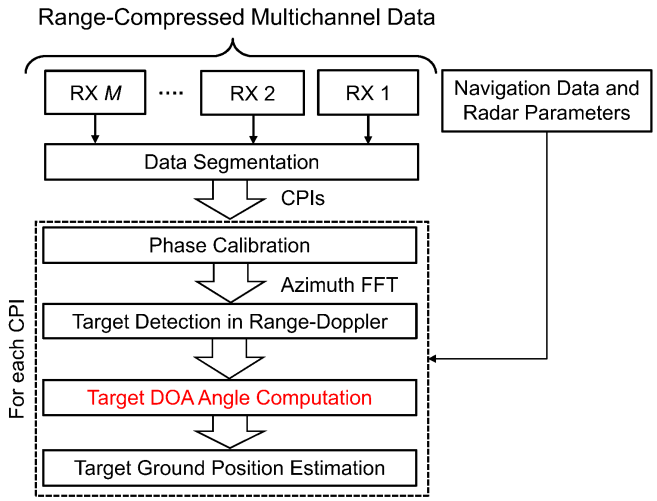

Fig. 2. Simplified flowchart of the radar-based maritime surveillance using multichannel airborne radar data. The DOA angle estimation block (shown in red) is the focus of this letter.

This letter proposes four methods for estimating the DOA angle of extended targets. The estimated DOA angles using the proposed methods are further utilized for calculating the geographical positions of the targets. The computed geographical positions of the targets are then compared with the simultaneously acquired AIS-based ground truth data. Real moving ships in real multichannel airborne radar data acquired with the DLR's digital beamforming synthetic aperture radar (DBFSAR) system [8] are used for evaluating the proposed methods.

II. Multichannel Radar Data Processing

A simplified multichannel airborne radar data processing chain for target geolocation is shown in Fig. 2.

The algorithm operates on multichannel range-compressed airborne radar data. The multichannel data are initially partitioned into smaller coherent processing intervals (CPIs) along the azimuth direction. The length of the CPI is system parameter dependent. As an example, for the DBFSAR data, we use 128 consecutive temporal azimuth samples in a single CPI. Thus, with the pulse repetition frequency of 3 kHz, each CPI has a duration of approximately 43 ms. The CPIs are then calibrated for correcting the phase offsets among the RX channels. Correcting these offsets is mandatory for estimating accurately the target positions on ground [9]. After calibration, individual CPIs are then transformed into range-Doppler domain via azimuth fast Fourier transform (FFT).

The targets are detected in the range-Doppler domain, where after detection, their respective slant ranges are measured [6]. The main advantage of using the Doppler domain is that targets even with low radar-cross section moving with a certain LOS velocity appear out of the clutter region, thus improving their detectability.

Once a target is detected, its DOA angle is estimated via a beamforming operation. With the estimated DOA angle, the measured slant range, the known terrain elevation, and the known geographical aircraft position and attitude angles, the target position on ground can directly be computed.

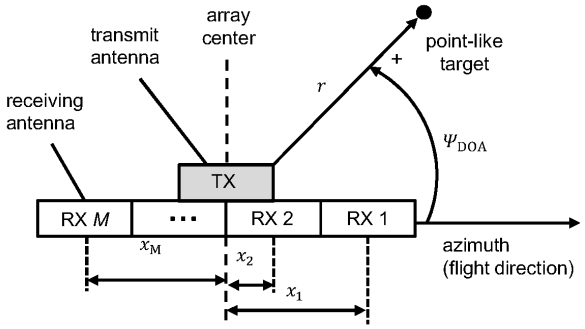

Fig. 3. Multichannel data acquisition geometry with M RX channels. The target range r and its corresponding DOA angle ψ_{DOA} are shown in the figure.

III. State-of-the-Art DOA Estimation for Point-Like Targets

In this section, we assume a point-like target for estimating the DOA angle. Fig. 3 shows the multichannel data acquisition geometry with the target of interest.

As shown in Fig. 3, the data are acquired using an antenna array with M RX channels arranged along the azimuth or flight direction. The multichannel signal model in expressed as [10]

$$s(t) = a_{\mathrm{s}} e^{-j\frac{4\pi}{\lambda}r(t)} D_{\mathrm{t}}(u(t)) \begin{bmatrix} D_{\mathrm{r},1}(u(t)) e^{j\frac{2\pi}{\lambda}u(t)x_1} \\ D_{\mathrm{r},2}(u(t)) e^{j\frac{2\pi}{\lambda}u(t)x_2} \\ \vdots \\ D_{\mathrm{r,M}}(u(t)) e^{j\frac{2\pi}{\lambda}u(t)x_{\mathrm{M}}} \end{bmatrix} = a_{\mathrm{s}} e^{-j\frac{4\pi}{\lambda}r(t)} \boldsymbol{d}(u(t)) \in \mathbb{C}^{M\times 1} \tag{1}$$

where a_{s} is the complex amplitude that comprises the reflectivity of the scatterer, λ is the radar wavelength, and $r(t)$ is the slant range between the target and the array center. The complex values $D_{\mathrm{t}}(u)$ and $D_{\mathrm{r,m}}(u)$ are the transmit and receive characteristics of the mth RX channel, x_{m} is the position of the antenna phase center in azimuth direction with respect to the array origin (cf. Fig. 3), and $\boldsymbol{d}(u)$ is the beamforming vector. The directional cosine u with respect to the antenna array can be expressed as a function of Doppler frequency f_{a} and the LOS velocity v_{r} of the target as [10]

$$u(f_{\mathrm{a}}, v_{\mathrm{r}}) = \cos(\psi_{\mathrm{DOA}}) = \frac{\lambda f_{\mathrm{a}}}{2v_{\mathrm{p}}} + \frac{v_{\mathrm{r}}}{v_{\mathrm{p}}} \tag{2}$$

where ψ_{DOA} is the DOA angle measured with respect to the antenna array and v_{p} is the platform velocity.

For calculating the DOA angle, the directional cosine of the target with respect to the antenna array is estimated using [3]

$$\hat{u} = \underset{u}{\operatorname{argmax}} \left| \boldsymbol{d}^H(u) \hat{\boldsymbol{R}}_{\mathbf{W}}^{-1}(f_{\mathrm{a}}) \boldsymbol{Z}(r, f_{\mathrm{a}}) \right|^2 \tag{3}$$

where $(\cdot)^H$ is the Hermitian operator (conjugate transpose) and $\hat{\boldsymbol{R}}_{\mathbf{W}}(f_{\mathrm{a}})$ is the clutter covariance matrix. The term $\boldsymbol{Z}(r, f_{\mathrm{a}})$ denotes the target's multichannel data vector at slant range r and Doppler frequency f_{a}.

When the targets are expected to have high signal-to-clutter-plus-noise ratio (SCNR), they can be detected without performing any clutter suppression. Therefore, the term $\hat{\boldsymbol{R}}_{\mathbf{W}}(f_{\mathrm{a}})$

shown in (3) can be omitted and the directional cosine of the target can be rewritten as

$$\hat{u} = \underset{u}{\operatorname{argmax}} \left| \boldsymbol{d}^H(u) \boldsymbol{Z}(r, f_a) \right|^2. \tag{4}$$

We use this simpler equation for avoiding any biases on the performance assessment caused by clutter suppression. The DOA angle of the target is then computed as

$$\hat{\psi}_{\mathrm{DOA}} = \cos^{-1}(\hat{u}). \tag{5}$$

IV. Proposed DOA Estimation Methods for Extended Targets

In this section, four different methods for estimating a single representative DOA angle of an extended target are presented. All point-like target detections of the extended target are combined in different ways, first for being able to provide an object-based position estimation at all and, second, for improving the geocoding accuracy. The goal is to have a single representative position for each extended target which, e.g., can be used later on for tracking purposes, as described in [2] and [8].

After detecting and clustering several pixel-based detections of a single target, the complex pixels belonging to the target are arranged as $\{\boldsymbol{Z}(r_1, f_{a1}), \boldsymbol{Z}(r_2, f_{a2}), \ldots, \boldsymbol{Z}(r_N, f_{aN})\}$, where N is the number of target-originated pixels in a cluster (cf. Fig. 1 where N is more than 4000).

For an extended target consisting of a given set of complex pixels, the single DOA angle is computed based on: 1) the average complex amplitude (ACA); 2) the maximum of the absolute amplitude (MAA); 3) the complex amplitude at the nearest neighbor to the center of gravity (NNCG) of the cluster; and 4) the mean DOA angle of the target pixels. For the first three methods, their respective complex signals that are used to estimate a single DOA angle for an extended target are expressed as

$$\boldsymbol{Z}_{\mathrm{ACA}}(r, f_a) = \frac{1}{N} \sum_{n=1}^{N} \boldsymbol{Z}(r_n, f_{an}) \tag{6}$$

$$\boldsymbol{Z}_{\mathrm{MAA}}(r, f_a) = \max \left| \{\boldsymbol{Z}(r_n, f_{an})\}_{n=1}^{N} \right| \tag{7}$$

$$\boldsymbol{Z}_{\mathrm{NNCG}}(r, f_a) = \boldsymbol{Z}(r_{\mathrm{NNCG}}, f_{\mathrm{NNCG}}) \tag{8}$$

where r_{NNCG} and f_{NNCG} are the range and Doppler positions of the NNCG pixel. By inserting independently the LHS variables of the (6)–(8) in (4), the directional cosine is obtained, and finally, the DOA angle of the target can be computed using (5).

For the fourth method, the DOA angle of the extended target is estimated as

$$\bar{\psi}_{\mathrm{DOA}} = \frac{1}{N} \sum_{n=1}^{N} \hat{\psi}_{\mathrm{DOA_n}} \tag{9}$$

where $\bar{\psi}_{\mathrm{DOA}}$ is the mean DOA angle of the target and $\hat{\psi}_{\mathrm{DOA_n}}$ is the DOA angle of the nth target pixel, which is computed by using (5).

An example is shown in Fig. 1, where the four aforementioned methods are used for estimating the geographical position of the ship HAM 316 at a specific time instant. It can be seen from the figure that the estimated ground positions of the ship are different because, for each method, the computed DOA angle is different. In Section VI, the accuracy of the estimated target ground positions achieved by these methods is evaluated and discussed in detail.

TABLE I

Radar System and Acquisition Geometry Parameters of the Real X-Band VV Polarized Multichannel Airborne Data Used for the Investigations

Acquisition Parameters	Typical Values		
	Data Set I	Data Set II	Data Set III
Average platform velocity [m/s]	90.9	90.5	84.9
Average platform altitude above ground [m]	2469.7	2465.3	2468.6
Aircraft course angle [°]	135	282	235-358
Number of TX/RX channels	1/4		
Physical antenna separation [m]	0.2		
Chirp bandwidth [MHz]	500		
Range resolution [m]	0.3		
Radar wavelength [m]	0.0309		
Pulse repetition frequency [Hz]	3004.8		
Total data acquisition time [s]	70	270	210

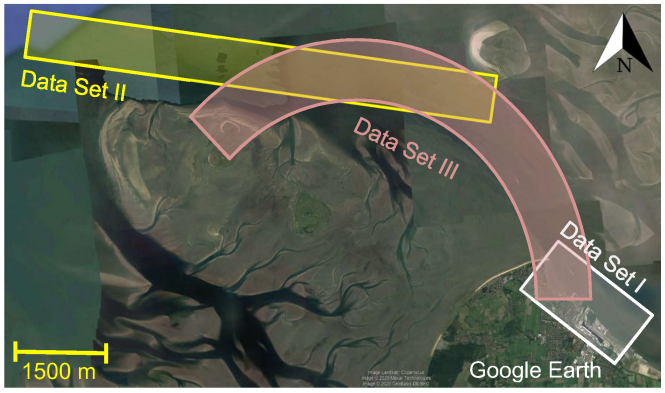

Fig. 4. Google Earth image showing the test site in North Sea near Cuxhaven, Germany. The datasets marked in the figure are described in Table I.

V. Experimental Setup and Datasets

In November 2019, a flight campaign with DLR's multichannel airborne radar system DBFSAR [8] was conducted in the North Sea near Cuxhaven, Germany. The aircraft was flying at an altitude of approximately 2400 m above ground. A dual-channel AIS receiver onboard the aircraft received the AIS signals from ships located up to 200 km away from the aircraft. The acquisition geometry and the system parameters of the acquired radar data are listed in Table I.

Fig. 4 shows the Google Earth image of the test site where the flight experiments were carried out. In the figure, datasets I and II were acquired using linear flight tracks (in strip map mode) and the dataset III was acquired using a circular flight track to observe a semi-annulus region (cf. aircraft's course angle in Table I).

VI. Experimental Results and Discussion

According to the received AIS messages, there were in total three ships in dataset I, nine ships in dataset II, and six ships in dataset III (cf. Table II). All the ships were successfully detected and tracked using the algorithm proposed

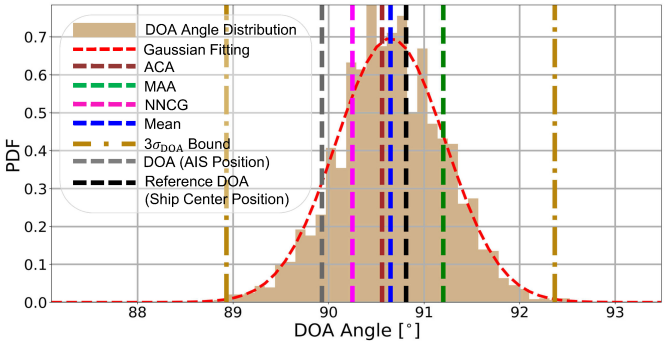

Fig. 5. Normalized histogram of the DOA angles estimated from the ship HAM 316 (cf. Fig. 1) in a single CPI. In the figure, the DOA angles estimated using the four methods, the DOA angles based on the AIS position and the ship center position are shown.

in [6] and [4]. The tracked ships are mapped on ground by using the DOA angles estimated with the proposed methods. For position accuracy assessment the actual geographical ship center position (cf. green dot in Fig. 1) is used as ground truth. This ship center position is derived from the AIS data by taking into account the known ship dimensions (yellow border in Fig. 1) and the known location of onboard GPS antenna (red dot in Fig. 1). Furthermore, for generating the results, the ship center positions are interpolated, since the time corresponding to the ship's center position do not usually match with the CPI center time of the radar acquisition.

Fig. 5 shows the probability density function (PDF) of the DOA angles for the ship HAM 316 (cf. Fig. 1 and dataset I in Table II) obtained from a single CPI, together with the DOA angles computed using the methods proposed in Section IV. The reference DOA angle in Fig. 5 (dashed black line) is calculated using the known reference ship center position and the position of the aircraft at the same azimuth time in the coordinate system whose x-axis is parallel to the aircraft's flight direction. From the figure it can be seen that the DOA angles seemingly follow a Gaussian distribution. In addition, the DOA angles estimated using the four methods, the DOA angle estimated from the AIS position, and the reference DOA angle estimated from the ship center position are all within the $\pm 3\sigma_{\text{DOA}}$ limit of the distribution.

For the assessment of the proposed DOA angle estimation methods, the target's DOA angle difference, the azimuth position difference, and the RMSE (root mean square error) of the target absolute position on ground are used as performance metrics. The DOA angle difference $\Delta\psi_{\text{DOA}}$ is computed between the estimated and the reference DOA angles of the target. The DOA angle difference is further used for computing the target's azimuth position difference Δx_{az} which is expressed as

$$\Delta x_{\text{az}} = r_{\text{et}} \cdot \sin(\Delta\psi_{\text{DOA}}) \tag{10}$$

where the term r_{et} is the slant range of the extended target, which is chosen based on the proposed method. For instance, for the MAA method [cf. (7)], the r_{et} corresponding to the peak absolute amplitude is selected. Fig. 6 top and center show $\Delta\psi_{\text{DOA}}$ and Δx_{az} estimates over several CPIs for the ship AURORA (cf. dataset III in Table II), respectively.

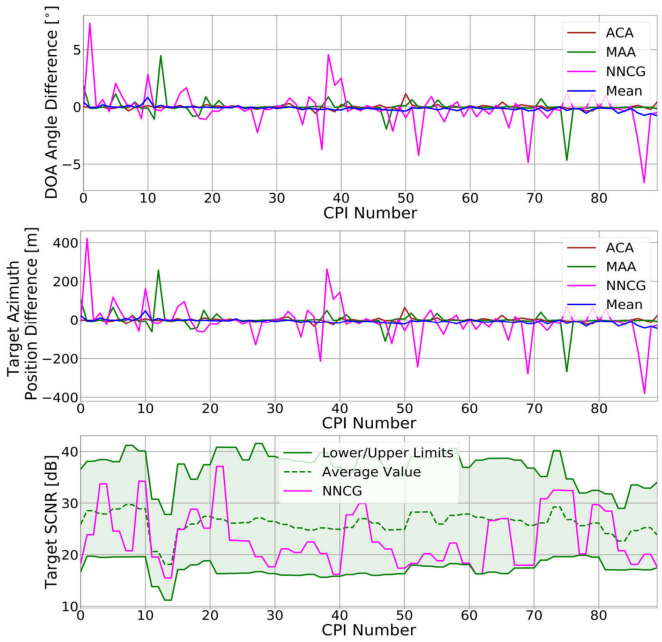

Fig. 6. Ship AURORA: (Top) DOA angle difference, (center) its corresponding azimuth position difference, and (bottom) its SCNR band over CPI.

For Fig. 6 top the average DOA angle differences obtained using the ACA, MAA, NNCG, and the mean DOA methods are 0.12°, 0.28°, 1.03°, and 0.18°, respectively. Their corresponding average azimuth position differences are calculated as 7.06, 16.22, 59.73, and 10.77 m, respectively. For the methods based on MAA and NNCG, the DOA angle and the azimuth position differences are the highest. This is because the DOA angles calculated for these methods are based on the phase derived from a single pixel. Such a phase value is susceptible to a high additive phase noise component that can bias the estimated DOA angle and, hence, the ground position accuracy of the extended target, especially under low SCNR conditions which may occur due to small aspect angle change.

On the other hand, for the method based on ACA, the DOA angle is estimated after averaging the complex amplitude pixels of the target. By averaging, it is expected that the phase fluctuations among the detected target pixels is significantly reduced and thus, the estimated DOA angle is improved as shown by the brown curve in Fig. 6 top. For the method based on the mean DOA angle, it can be seen that, like the ACA-based method, the estimated DOA angles and the azimuth position differences also show low fluctuations. However, it is pointed out here that if an individual CPI contain thousands of detected target pixels, as shown in Fig. 1, the ACA-based method can be up to thousand times faster than the mean DOA angle method. This is because, for the latter method, the beamforming and, hence, the DOA angle is estimated for each detected target pixel [cf. (4)] and for the ACA-based method, beamforming is performed only once, i.e., on the average complex target amplitude only. Therefore, the method based on the mean DOA angle is not suitable for real-time applications.

Finally, the target's absolute ground position errors are calculated for all 18 ships considered in this letter. The results

TABLE II

RMSE ASSESSMENT OF THE ABSOLUTE GROUND POSITIONS OF ALL THE SHIPS IN THE MULTICHANNEL DATASETS USING THE PROPOSED DOA ANGLE ESTIMATION METHODS. THE NUMBERS IN BOLD SHOW THE BEST ACCURACY ACHIEVED WITH THE PROPOSED METHODS. TRACKING TIME AND THE TARGET AVERAGE SCNR VALUES ARE SOME ADDITIONAL INFORMATION OF THE SHIPS OBTAINED AFTER TRACKING [4]. IN THE TABLE, THE LISTED SHIP DIMENSIONS AND THEIR RESPECTIVE MOVING DIRECTIONS ARE BASED ON THE RECEIVED AIS MESSAGES

	Absolute Ground Position Error [m]				Tracking Time [s]	Target Average SCNR [dB]	Ship Length/Beam [m]	Ship Moving Direction w.r.t the Aircraft [°]
	ACA	MAA	NNCG	Mean				
Ship Name					Data Set I			
LANGELAND	27.27	62.17	110.47	**12.22**	4.31	28.76	82/12	-8.35
LONGDUIN	34.83	35.91	59.79	**11.82**	2.85	19.32	112/15	195.93
HAM 316	37.44	51.34	159.92	**27.55**	4.25	27.71	129/22	-1.23
					Data Set II			
CHARISMA	15.98	41.71	89.76	**12.32**	4.72	23.45	12/4	7.67
HOFFNUNG CUX10	**11.91**	48.33	80.79	14.44	4.85	22.16	15/5	-0.32
SAPHIR	9.21	38.82	98.08	**6.67**	5.49	29.11	17/6	1.59
GEO GRAPH	17.39	32.31	69.29	**13.43**	4.13	25.18	18/6	-150.48
UTHOERN	11.39	24.67	86.42	**6.05**	4.13	27.43	31/9	-182.02
WANGEROOGE	14.22	52.21	52.86	**11.86**	3.96	25.35	52/13	20.14
FAIR LADY	30.03	66.38	129.65	**28.13**	6.62	32.35	68/10	4.39
MT BLUE STAR	111.54	**98.63**	166.17	100.93	4.68	28.64	126/18	23.31
VEGA GRANAT	69.02	58.18	135.95	**37.05**	4.17	31.03	180/20	-169.94
					Data Set III			
GEO GRAPH	14.66	64.31	126.49	**12.18**	4.04	28.55	18/6	-11.81
TINA CUX-5	**17.35**	50.99	144.35	19.65	4.72	25.64	19/5	-173.52
AURORA	**13.52**	45.06	110.19	17.33	4.04	26.07	20/6	-104.68
PILOTVESSEL HANSE	**23.08**	106.84	109.24	42.97	3.45	31.93	49/21	-182.36
RMS RATINGEN	**32.82**	53.03	140.59	33.25	3.49	33.25	88/11	-185.16
LONGDUIN	48.93	54.05	188.77	**26.03**	3.79	30.11	112/15	-3.75
Overall Accuracy	30.03	54.72	114.38	**24.14**				

are shown in Table II. As shown in the table, the methods based on the mean DOA angle and the ACA are the best ones, achieving an overall position accuracy of 24 and 30 m, respectively. Such accuracy for an extended target can be considered very good for radar-based ship monitoring using an airborne radar sensor.

VII. CONCLUSION

This letter presents and compares four methods for estimating the DOA angle of extended targets using high resolution range-compressed multichannel airborne radar data. The methods are evaluated using three real X-band VV polarized radar datasets (two linear and one circular flight) acquired with the DLR's DBFSAR system, in which ships with different dimensions and moving directions are contained. Based on the experimental results, we recommend using the ACA method for estimating the DOA angles of extended targets. This method allows not only for achieving an acceptable position accuracy, but it is also computationally efficient and has real-time processing capability.

REFERENCES

[1] A. N. Ince, E. Topuz, E. Panayirci, and C. Isik, *Principles of Integrated Maritime Surveillance Systems*, vol. 527. Cham, Switzerland: Springer, 2012.

[2] S. V. Baumgartner and S. K. Joshi, "Promising techniques for future maritime surveillance demonstrated with DLR's airborne radar sensors F-SAR and DBFSAR," in *Proc. ESA Adv. RF Sensors Remote Sens. Instrum. (ARSI)*, Nov. 2019, pp. 1–6.

[3] D. Cerutti-Maori, J. Klare, A. R. Brenner, and J. H. G. Ende, "Wide-area traffic monitoring with the SAR/GMTI system PAMIR," *IEEE Trans. Geosci. Remote Sens.*, vol. 46, no. 10, pp. 3019–3030, Oct. 2008.

[4] S. K. Joshi, S. V. Baumgartner, and G. Krieger, "Tracking and track management of extended targets in range-Doppler using range-compressed airborne radar data," *IEEE Trans. Geosci. Remote Sens.*, vol. 60, pp. 1–20, 2022.

[5] M. Mertens and R. Kohlleppel, "Ground target tracking with experimental data of the PAMIR system," in *Proc. 17th Int. Conf. Inf. Fusion (FUSION)*, Jul. 2014, pp. 1–8.

[6] S. K. Joshi, S. V. Baumgartner, A. B. C. da Silva, and G. Krieger, "Range-Doppler based CFAR ship detection with automatic training data selection," *Remote Sens.*, vol. 11, no. 11, p. 1270, May 2019.

[7] C. Kuang, C. Wang, B. Wen, and W. Huang, "An applied method for clustering extended targets with UHF radar," *IEEE Access*, vol. 8, pp. 98670–98678, 2020.

[8] A. Reigber *et al.*, "The high-resolution digital-beamforming airborne SAR system DBFSAR," *Remote Sens.*, vol. 12, no. 11, p. 1710, May 2020.

[9] A. B. C. da Silva, S. K. Joshi, S. V. Baumgartner, F. Q. de Almeida, and G. Krieger, "Phase correction for accurate DOA angle and position estimation of ground-moving targets using multi-channel airborne radar," *IEEE Geosci. Remote Sens. Lett.*, vol. 19, pp. 1–5, 2022.

[10] J. H. G. Ender, C. H. Gierull, and D. Cerutti-Maori, "Improved space-based moving target indication via alternate transmission and receiver switching," *IEEE Trans. Geosci. Remote Sens.*, vol. 46, no. 12, pp. 3960–3974, Dec. 2008.